Nonlinear Analysis: Modelling and Control, 2002, Vol. 7, No. 2, 15–36

Controlling Chaos and Bifurcation of Subsynchronous Resonance in Power System

A.M. Harb, M.S. Widyan

Department of Electrical Engineering
Jordan University of Science and Technology
P.O.Box 3030, Ibid, Jordan

aharb@just.edu.jo

Received: date 26.06.2002
Accepted: date 13.11.2002

Abstract. Linear and nonlinear state feedback controllers are proposed to control the bifurcation of a new phenomenon in power system, this phenomenon of electro-mechanical interaction between the series resonant circuits and torsional mechanical frequencies of the turbine generator sections, which known as Subsynchronous Resonance (SSR). The first system of the IEEE second benchmark model is considered. The dynamics of the two axes damper windings, Automatic Voltage Regulator (AVR) and Power System Stabilizer (PSS) are included. The linear controller gives better initial disturbance response than that of the nonlinear, but in a small narrow region of compensation factors. The nonlinear controller not only can be easily implemented, but also it stabilizes the operating point for all values of the bifurcation parameter.

Keywords: subsynchronous resonance, power system, control of chaos.

1 Introduction

The phenomenon of SSR has been studied very extensively since 1970 when a major transmission network in the USA experienced shaft failure to its T-G unit with series compensation in the 500KV lines. This has now gone into technical literature as a classical problem and known as Project Navajo. However, this phenomenon had been known to exist for a few years according to many experts who predicted such a phenomenon in series-compensated lines connected to T-G units [1]. In fact, series compensation has been considered as a powerful alternative based on economic and technical considerations for increasing

effectively the power transfer capability and improving the stability of extra high voltage systems.

In the last few years, power system dynamics have been studied from nonlinear dynamics point of view using bifurcation theory. In fact, power system has rich bifurcation phenomena. Particularly, when the consumer demand for reactive power reaches its peaks, the dynamics of an electric power network may move to its stability margin, leading to oscillations and bifurcations.

SSR is a phenomenon in power system in which bifurcation theory can be applied. The most commonly encountered bifurcation is the dynamic bifurcation "Hopf bifurcation" in which a complex conjugate pair of eigenvalues of the linearized model around the operating condition transversally crosses the imaginary axis of the complex plane. The birth of limit cycle from an equilibrium point gives rise to oscillations, which may undergo complicated bifurcations such as period multiplication, cyclic folds or crises. Zhu *et al.* [2] used the Hopf bifurcation theorem, in which the dynamics of the AVR and damper windings are neglected, to study a SMIB power system experienced SSR, a prediction of supercritical Hopf bifurcation is investigated. The bifurcation analysis is used by Nayfeh *et al.* [3] to investigate the complex dynamics of a heavily loaded SMIB power system modeling the characteristics of the BOARDMAN generator with respect to the rest of the North-Western American Power System. In their study, the dynamic effects of d- and q-axes damper windings are included while that of the AVR is neglected. The results show that, as the compensation factor increases the operating point loses stability via supercritical Hopf bifurcation. On further increase of the compensation factor the system route to chaos via torus breakdown. Also it is concluded that the effect of the damper windings on that system is to destabilize the system by reducing the compensation level at which SSR occurs. The effect of electrical machine saturation on SSR is also studied by Harb *et al.* [4]; they concluded that, the generator saturation slightly shrinks the positively damped region by shifting the Hopf bifurcation point to smaller compensation level. It also slightly shifts the secondary Hopf bifurcation and blue sky catastrophe to smaller compensation level.

Bifurcation control deals with modification of bifurcation characteristics of a parameterized nonlinear system by a designed control input. Typical

bifurcation control objectives include delaying the onset of an inherent bifurcation [5] and [6], introducing a new bifurcation at a preferable parameter value [7] and [8], changing the parameter value of an existing bifurcation point [9] and [10], modifying the shape or type of a bifurcation chain [6], stabilizing a bifurcated solution or branch [11] and [12], monitoring the multiplicity [13], amplitude [14], and/or frequency of some limit cycles emerging from bifurcation [15] and optimizing the system performance near a bifurcation point [16].

Bifurcation control with various objectives have been implemented in experimental systems or tested by using numerical simulations in a great number of engineering, biological, and physicochemical systems; examples can be named in chemical engineering [17] and [18], mechanical engineering [19]–[21], electrical engineering [22]–[28], biology [29], physics and chemistry [30]–[32] and meteorology [33]. Bifurcation control is not only important in its own right, but also suggests a viable and effective strategy for chaos control, this because the bifurcation and chaos are usually twins.

It is now known that bifurcation properties of a system can be modified via various feedback control methods. Representative approaches employ linear or nonlinear state-feedback controls [8], [11], [34] and [35], apply a washout filter-aided dynamic feedback controller [35], and use harmonic balance approximations [10].

The aims of the paper are to use linear and nonlinear controllers to control bifurcation and chaos of SSR for the IEEE second benchmark model, and to compare between these two types of controllers.

The paper is organized as follows: In section 2, a description of the considered system is given. Section 3 gives the mathematical model of the open loop system. Section 4 discussed the used linear and nonlinear state feedback controllers. Numerical simulation results for both open and closed loop systems are given in section 5, and finally some conclusions are withdrawn in section 6.

2 System Description

After Harb & Widyan [36], we considered the first system of the IEEE second benchmark models of subsynchronous resonance. As shown in fig. 1, it is a

SMIB power system with two transmission lines, one of them is compensated by a series capacitor.

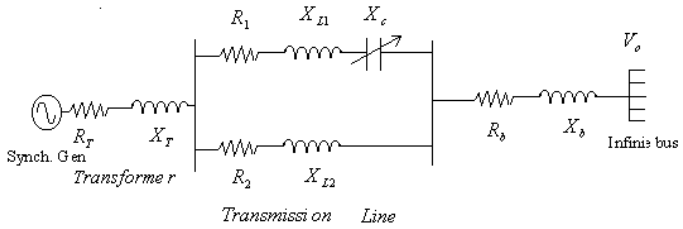

Fig. 1. Power system under study
(System 1, IEEE Second Benchmark Model of SSR)

Fig. 2 shows the automatic voltage regulator (AVR) that controls the excitation voltage of the synchronous generator with the terminal voltage of synchronous generator as an input signal, while the output signal is the d-axis field voltage, and power system stabilizer (PSS) that uses auxiliary (supplementary) stabilizing signals to control the excitation system so as to improve power system dynamic performance.

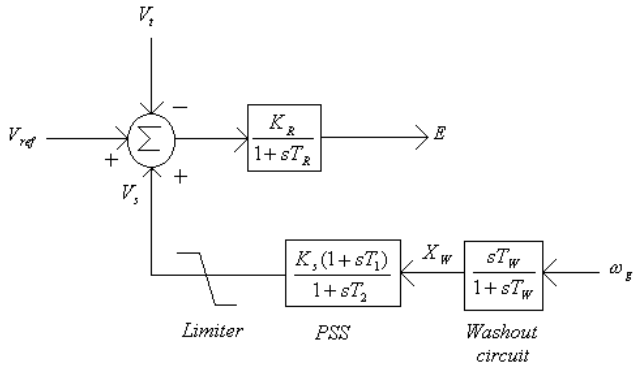

Fig. 2. Block diagram of the used AVR and PSS

3 Mathematical Model

Using direct, quadrature (*d*- and *q*-axes) and Park's transformation, the complete mathematical model that describes the dynamics of the system can be found in [36]:

a) Synchronous Generator:

$$X_{ffd}\frac{di_{fd}}{dt} - X_{afd}\frac{di_d}{dt} + X_{fkd}\frac{di_{kd}}{dt} = \omega_o \frac{r_{fd}}{X_{afd}} E - \omega_o r_{fd} i_{fd}\,, \tag{1}$$

$$\begin{aligned} X_{afd}\frac{di_{fd}}{dt} - (X_d + X_T + kX_{L1} + X_b)\frac{di_d}{dt} + X_{akd}\frac{di_{kd}}{dt} \\ = \omega_o V_o \sin\delta_g + \omega_o (R_b + R_T + kR_1 + r_a) i_d \\ - \omega_o (X_T + X_b + kX_{L1} + + \omega_g X_q) i_q + \omega_o \omega_g X_{akq} i_{kq} + \omega_o v_{cd}\,, \end{aligned} \tag{2}$$

where $k = \dfrac{\sqrt{R_2^2 + X_{L2}^2}}{\sqrt{(R_1 + R_2)^2 + (X_{L1} + X_{L2} - \mu X_{L1})^2}}$,

$$X_{fkd}\frac{di_{fd}}{dt} - X_{akd}\frac{di_d}{dt} + X_{kkd}\frac{di_{kd}}{dt} = -\omega_o r_{kd} i_{kd}\,, \tag{3}$$

$$\begin{aligned} -(X_q + X_T + kX_{L1} + X_b)\frac{di_q}{dt} + X_{akq}\frac{di_{kq}}{dt} \\ = \omega_o V_o \cos\delta_g - \omega_o \omega_g X_{afd} i_{fd} + \omega_o (X_T + X_b + kX_{L1} + \omega_g X_d) i_d \\ - \omega_o \omega_g X_{akd} i_{kd} + \omega_o (R_T + R_b + kR_1 + r_a) i_q + \omega_o v_{cq}\,, \end{aligned} \tag{4}$$

$$-X_{akq}\frac{di_q}{dt} + X_{kkq}\frac{di_{kq}}{dt} = -\omega_o r_{kq} i\,. \tag{5}$$

b) Transmission Line:

With $X_c = \mu X_{L1}$,

$$\frac{dv_{cd}}{dt} = \omega_o \mu k X_{L1} i_d - \omega_o v_{cq}\,, \tag{6}$$

$$\frac{dv_{cq}}{dt} = \omega_o \mu k X_{L1} i_q - \omega_o v_{cd}\,. \tag{7}$$

c) Mechanical System:

$$\frac{d\delta_1}{dt} = \omega_o \omega_1 - \omega_0\,, \tag{8}$$

$$M_1\frac{d\omega_1}{dt} = D_1 - D_1\omega_1 - K_{1g}\delta_1 + K_{1g}\delta_g\,, \tag{9}$$

$$\frac{d\delta_g}{dt} = \omega_o \omega_g - \omega_o , \tag{10}$$

$$\begin{aligned} M_g \frac{d\omega_g}{dt} = {} & T_m + D_g - X_{afd} i_q i_{fd} + X_d i_q i_d \\ & - X_{akd} i_{kd} i_q - X_q i_q i_d + X_{akq} i_{kq} i_d - D_g \omega_g \\ & + K_{1g} \delta_1 - K_{1g} \delta_g - K_{g2} \delta_g + K_{g2} \delta_2 , \end{aligned} \tag{11}$$

$$\frac{d\delta_2}{dt} = \omega_o \omega_2 - \omega_o , \tag{12}$$

$$M_2 \frac{d\omega_2}{dt} = D_2 - D_2 \omega_2 + K_{g2} \delta_g - K_{g2} \delta_2 - K_{23} \delta_2 + K_{23} \delta_3 , \tag{13}$$

$$\frac{d\delta_3}{dt} = \omega_o \omega_3 - \omega_o , \tag{14}$$

$$M_3 \frac{d\omega_3}{dt} = D_3 - D_3 \omega_3 + K_{23} \delta_2 - K_{23} \delta_3 . \tag{15}$$

d) Automatic Voltage Regulator (AVR) and Power System Stabilizer (PSS) Mathematical Model

The mathematical model of AVR and PSS (fig. 2) is given by the following equations:

$$T_W \frac{dX_W}{dt} - T_W \frac{d\omega_g}{dt} = -X_W , \tag{16}$$

$$T_2 \frac{dV_S}{dt} - T_1 K_s \frac{dX_W}{dt} = K_s X_W - V_s , \tag{17}$$

$$T_R \frac{dE}{dt} = K_R V_{ref} + K_R V_s - K_R V_t - E . \tag{18}$$

With $V_t = \sqrt{V_d^2 + V_q^2}$, neglecting stator transients yields:

$$V_d = -r_a i_d + X_q i_q ,$$

$$V_q = -r_a i_q - X_d i_d + X_{afd} i_{fd} .$$

Consequently,

$$V_t = \sqrt{(-r_a i_d + X_q i_q)^2 + (-r_a i_q - X_d i_d + X_{afd} i_{fd})^2} . \tag{19}$$

Hence, the system can be written in state space representation in the form:

$$\frac{dx}{dt} = F(x;\mu), \tag{20}$$

where μ is the bifurcation parameter, representing the compensation factor (X_c / X_{L1}) of the power system. In all cases, the system has more than one equilibrium solution; the selected one is the equilibrium, which represent the operating point resulting in a heavily loaded generator with $Pe = 0.9$, $Q_e = 0.43$ and $V_t = 1.138$ pu.

Equations (1)–(19) give a complete description to the dynamics of the SMIB power system with two transmission lines one of them is compensated by a series capacitor. The state variables are $x_1 = i_{fd}$, $x_2 = i_d$, $x_3 = i_{kd}$, $x_4 = i_q$, $x_5 = i_{kq}$, $x_6 = v_{cd}$, $x_7 = v_{cq}$, $x_8 = \delta_1$, $x_9 = \omega_1$, $x_{10} = \delta_g$, $x_{11} = \omega_g$, $x_{12} = \delta_2$, $x_{13} = \omega_2$, $x_{14} = \delta_3$, $x_{15} = \omega_3$, $x_{16} = X_W$, $x_{17} = V_s$ and $x_{18} = E$. All parameters are given in the Appendix.

4 Linear and Nonlinear State Feedback Controller

4.1 Linear State Feedback Controller. It is based on the linearized version around the operating point of the nonlinear dynamical system. The control is achieved by feeding back the state variables through a regulator with constant gains. Consider the following linearized version of a nonlinear system in the state-variable form [37]:

$$\frac{dx}{dt} = Ax + Bu, \tag{21}$$

where A is an $n \times n$ constant matrix and B is an $n \times m$ constant matrix, here m is the number of the system inputs, given by

$$A = \frac{\partial \dot{x}}{\partial x}, \quad B = \frac{\partial \dot{x}}{\partial u} \tag{22}$$

evaluated at the operating point.

Now consider the block diagram of the system shown in fig. 4 with the following state feedback control

$$u(t) = -Kx\,, \tag{23}$$

where K is a $m \times n$ matrix of constant feedback gains.

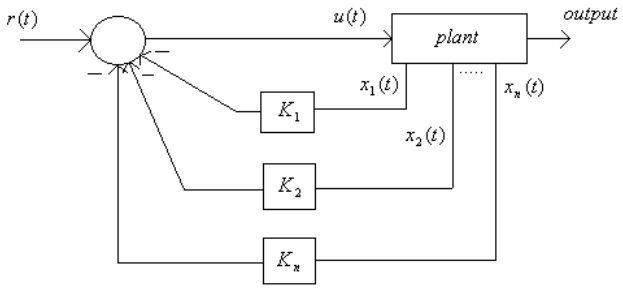

Fig. 4. Control system design via linear state feedback

The control system input $r(t)$ is assumed to be zero. The purpose of this system is to return all state variables to values of zero when the states have been perturbed. Substituting equation (23) into equation (21), the compensated system state-variable representation becomes

$$\dot{x} = (A - BK)x = A_f x\,. \tag{24}$$

The closed loop characteristic equation is

$$\left|sI - A + BK\right| = 0 \tag{25}$$

and for a specified closed-loop pole locations $\lambda_1, \lambda_2, ..., \lambda_n$, the design objective is to find the gain matrix K such that the characteristic equation of the closed loop system Equation (25) has the specified closed loop eigenvalues.

The necessary and sufficient condition, which enables us to place the closed-loop eigenvalues anywhere, is that the linearized system around the operating point is controllable, that is the controllability matrix has a full rank i.e.

$$\rho[B \quad AB \quad A^2B \ldots A^{n-1}B] = n\,. \tag{26}$$

4.2 Nonlinear State Feedback Controller. The considered nonlinear controller is of the form:

$$u = -K(\omega_g^3 - \omega_1^3)\,. \tag{27}$$

In this controller, just two state signals of the system must be measured, the rotor generator speed ω_g and the first turbine-generator section speed ω_1. Then ω_1^3 is subtracted from ω_g^3. Because $\omega_1 = \omega_g$ at steady state, the nonlinear controller will not affect the equilibrium solutions of the system, but it will affect the Jacobean matrix of the system, as a result the eigenvalues of the linearized model will be altered by this controller at different compensation factors. Then, the result is multiplied by a gain *K*, this gain must be carefully adjusted such that it will make a significant effect on the equilibrium stability of the system. fig. 5 shows the block diagram of the AVR and PSS together with the considered nonlinear feedback controller.

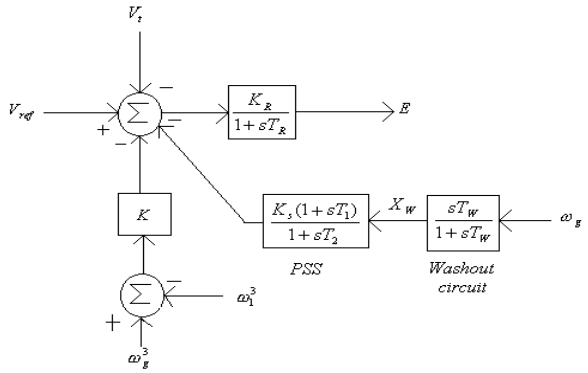

Fig. 5. AVR, PSS together with the considered nonlinear state feedback controller

5 Numerical Simulation Results

5.1 The case of linear state feedback controller. In this case, we consider the SMIB power system without taking the AVR and PSS into account, and it assumed that the only input to the system is the internal generated voltage. The study is carried out with heavily loaded synchronous generator of $P_e = 0.9$, $Q_e = 0.43$ and $V_t = 1.138$ at a compensation factor $\mu = 0.1$ by adjusting $E = 2.2$ and $T_m = 0.91$. First, the bifurcation theory is applied to the open loop system when the compensation factor μ varies from 0 up 1. This case is studied

in details by Harb and Widyan [36], in which we have 15 differential equations (1)–(15). The 15×15 Jacobean matrix is obtained and the stability of the operating point is studied by monitoring the eigenvalues of the linearized version.

Fig. 6 shows the variation of real and imaginary parts of the eigenvalues with the compensation factor μ. It can be observed that, for small μ the frequencies of the electrical modes are approximately 377 rad/sec. As μ increases they start separate from each other. The first one starts increasing and called supersynchronous, while the second starts decreasing and called subsynchronous electrical mode. The latter one is of prime interest because when it interacts with the torsional modes, they may be self excited and this is dangerous since, if this occurs, they will cause loss of fatigue life and eventually, the destruction of the rotor, even if they have small amplitudes.

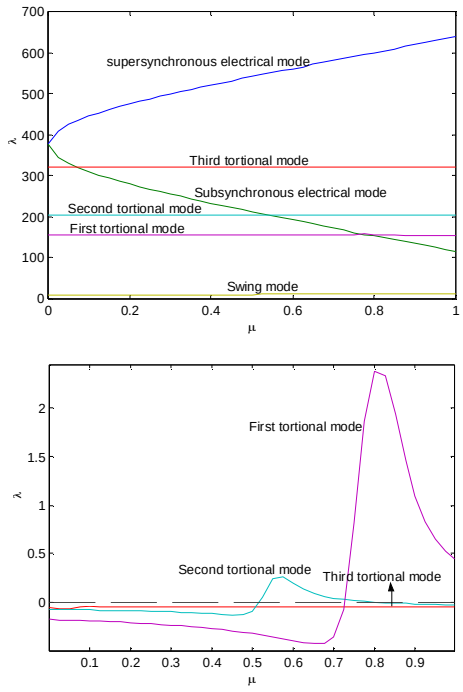

Fig. 6. Variation of real and imaginary parts of eigenvalues with the compensation factor μ

It is clear that at $\mu \approx 0.518429$, the subsynchronous electrical mode interacts with the second torsional mode resulting in moving of the

corresponding real parts of eigenvalues towards the zero axis. Unfortunately, this interaction was strong enough to transversally move the real parts of the corresponding eigenvalues from left- to the right half of the complex plane. Hence, a Hopf bifurcation had been occurred.

The bifurcation diagram is shown in fig. 7 in $\delta_g - \mu$ plane. It can be observed that, the power system has stable operating point in the region $0 < \mu < H \approx 0.518429$, unstable operating point in the region $H \approx 0.518429 < \mu \leq 1$ and a Hopf bifurcation point at $\mu = H \approx 0.518429$.

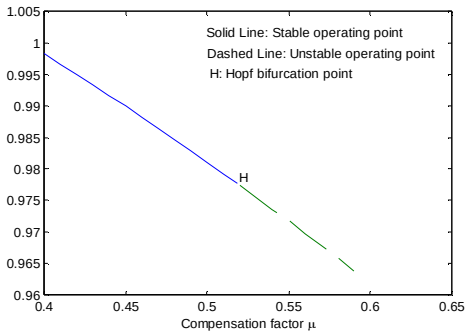

Fig. 7. Variation of rotor angle of generator with compensation factor (Bifurcation diagram, δ_g vs. μ)

A Hopf bifurcation point is that point at which the stationary equilibrium solution is connected to that of the periodic solution, thus at $\mu = H \approx 0.518429$, a limit cycle is born, this limit cycle is stable if the Hopf bifurcation is supercritical and unstable in case of sub critical Hopf bifurcation. The type of the Hopf bifurcation can be determined by either perturbation techniques based on the method of multiple scales or numerical method based on the response of the perturbed system. Harb & Widyan [36] show that the Hopf bifurcation is supercritical.

Fig. 8 shows the time history of the system emanated near the Hopf bifurcation point, the two-dimensional projection and the corresponding FFT at different compensation factors after the Hopf bifurcation value. It can be observed that the system routes to chaos via torus breakdown intermittency. Also on further increase of the compensation factor, the chaotic attractor collides with its basin boundary resulting in destruction of both the attractor as

well as the boundary in a dangerous discontinuous bifurcation called blue-sky catastrophe, so there is no bounded motion as shown in fig. 9.

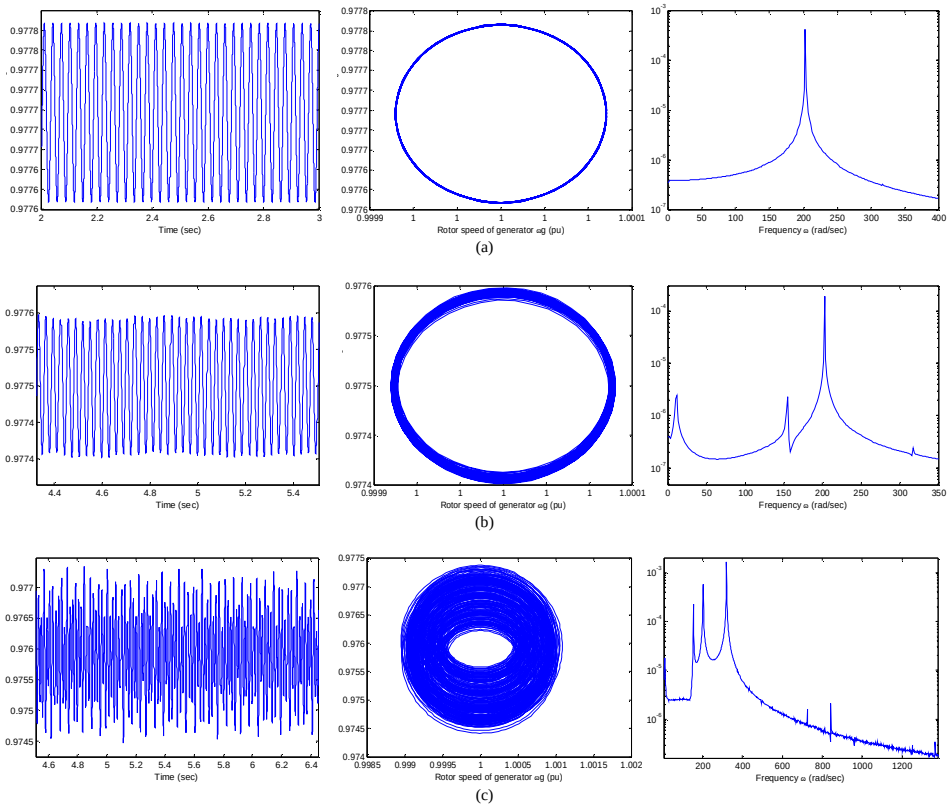

Fig. 8. Time histories of the rotor angle of generator (left), the corresponding two-dimensional projections of the phase portrait onto $\delta_g - \omega_g$ plane (middle), and the corresponding FFT (right). The solution at (a) limit cycle, (μ = 0.518429), (b) torus-attractor (μ = 0.519761) and (c) chaotic attractor, (μ = 0.527999)

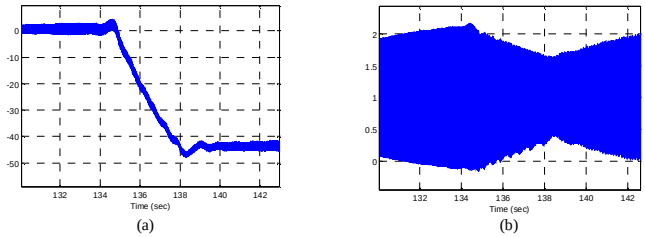

Fig. 9. Time history of (a) rotor angle of generator and (b) rotor speed of generator at μ = 0.528015 (blue-sky catastrophe)

Fig. 10 shows the open loop time history and the corresponding two-dimensional projection of the system at a compensation factor $\mu = 0.8$. It can be observed that the system has a chaotic behavior. So far all simulations were carried out without any control action. Next, a linear state feedback controller of the form:

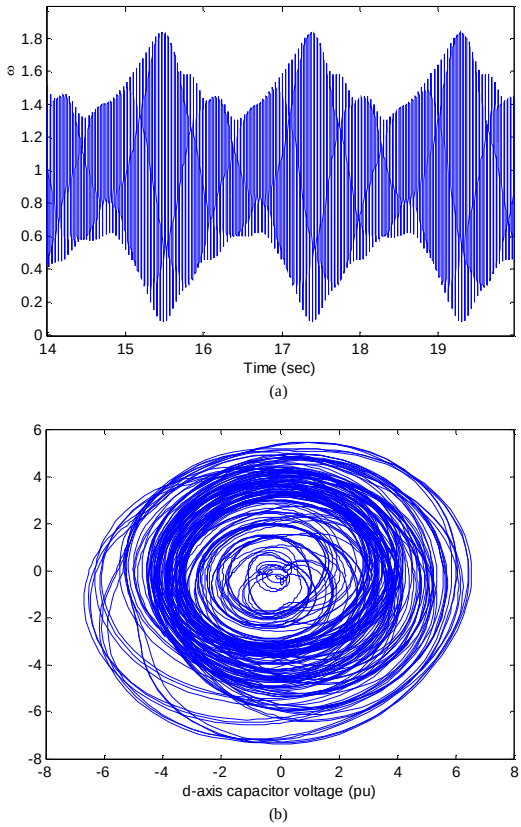

Fig. 10. (a) Open loop time history (Rotor speed of generator), (b) the corresponding two-dimensional projection (d-axis capacitor voltage vs. q-axis capacitor voltage) at $\mu = 0.8$

$$\begin{aligned} u = V_{ref} &- (K_1 i_{fd} + K_2 i_d + K_3 i_{kd} + K_4 i_q + K_5 i_{kq} \\ &+ K_6 v_{cd} + K_7 v_{cq} + K_8 \delta_1 + K_9 \omega_1 + K_{10} \delta_g \\ &+ K_{11} \omega_g + K_{12} \delta_2 + K_{13} \omega_2 + K_{14} \delta_3 + K_{15} \omega_3) \end{aligned} \tag{28}$$

is designed.

Now, the objective is to find the constant gains ($K_1 \ldots K_{15}$) such that the linearized model around the operating point has the desired eigenvalues of:

$$P = -12 \pm 600\text{i}, -5 \pm 321\text{i}, -4 \pm 204\text{i}, -12 \pm 155\text{i}, -6 \pm 160\text{i}, -30, \\ -5 \pm 11\text{i}, -5, -10.$$

The MATLAB built in function $K = place(A, B, P)$ is used to find the designed gains ($K_1 \ldots K_{15}$), and the following result is obtained

$$K_1 = 679.256, \quad K_2 = \text{-}696.885, \quad K_3 = 671.937, \quad K_4 = 396.004,$$
$$K_5 = \text{-}324.289, \quad K_6 = 342.566, \quad K_7 = 281.193, \quad K_8 = \text{-}23621.7,$$
$$K_9 = \text{-}19569.1, \quad K_{10} = 35635.9, \quad K_{11} = 34901.2, \quad K_{12} = 16693.8,$$
$$K_{13} = \text{-}30131.6, \quad K_{14} = 4886.87, \quad K_{15} = 13439.7.$$

Fig. 11 shows the response of the system based on the nonlinear model at a compensation factor $\mu = 0.8$ after 2.5% initial disturbance on the rotor speed of the generator when the linear state feedback controller is applied, it can be observed that the system has been stabilized by using this controller.

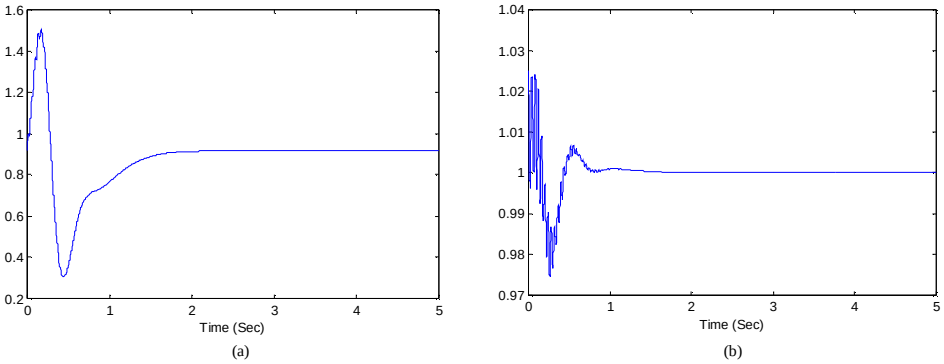

Fig. 11. Closed loop response (a) Rotor angle, and (b) Rotor speed of generator after 2.5% initial disturbance on the rotor speed of generator (with linear state feedback controller, at $\mu = 0.8$)

In order to keep an invariant eigenvalues of the linearized system at all compensation factors, and so to cancel all bifurcations of the system using

linear state feedback controller, one must vary the controller gains at all compensation factors, and before that one must check the controllability of the system at every compensation factor.

5.2 The case of nonlinear state feedback controller. In this subsection, the case of including the dynamics of the two axes damper windings, AVR and PSS. Before we mention the effect of the nonlinear state feedback controller, the effect of the AVR gain K_R (fig. 5) should be investigated. fig. 12 shows the location of the Hopf bifurcation point as a function of the AVR gain K_R, it can be observed that as the value of K_R decreases the Hopf bifurcation point increases or equivalent to say that the stability region increases.

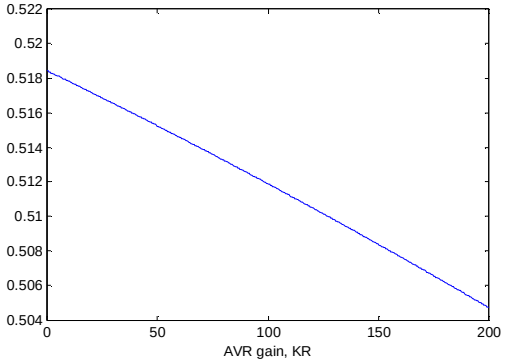

Fig. 12. Variation of Hopf bifurcation point H with AVR gain K_R

A nonlinear controller of the form of equation (27) has been designed. As we mentioned early, two state signals of the system must be measured, the rotor generator speed ω_g and the first turbine-generator section speed ω_1.

As down in the AVR gain, fig. 14 shows the variation of the Hopf bifurcation point H with the value of the nonlinear controller gain K when the AVR gain K_R is adjusted at a very small value of 2. It can be observed that, as the nonlinear controller gain increases, the Hopf bifurcation point increases so, the equilibrium stable region increases. Also it can be observed that, if one adjust the nonlinear state feedback gain to a value greater than 4500, then the operating point of the system will never loss stability at any compensation factor, so the system will never experience any bifurcations.

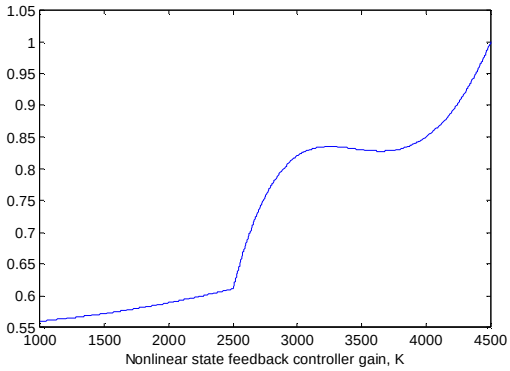

Fig. 14. Variation of Hopf bifurcation point *H* with the nonlinear state feedback controller gain *K* when AVR gain $K_R = 2$

Fig. 15 shows the variation of the real and imaginary parts of eigenvalues of the linearized system around the operating point with the compensation factor μ with nonlinear state feedback controller gain $K = 5000$ and AVR gain $K_R = 2$. It can be inferred that, despite the sub synchronous resonance mode interactions with the torsional mechanical modes, the operating point never lose stability at any compensation factor, so with nonlinear state feedback controller together with small amplitude AVR gain, the system operating point never lose stability.

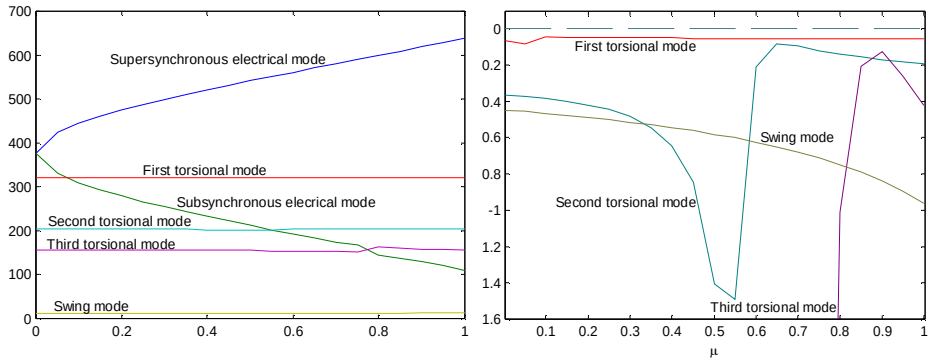

Fig. 15. Variation of real and imaginary parts of eigenvalues with μ (the case of nonlinear state feedback controller with gain K = 5000 and AVR gain K_R = 2)

Fig. 16 shows the time history of the system at compensation factor $\mu = 0.8$ in cases of no controllers and with the nominal value of AVR gain $K_R = 200$. It can be inferred that the operating point of the system is unstable.

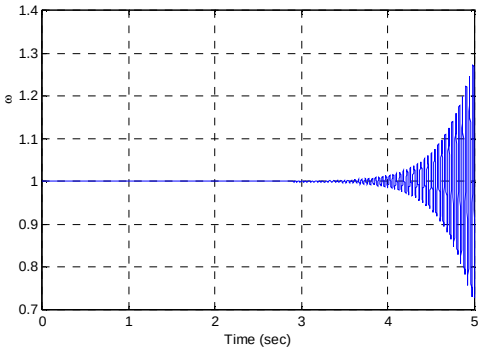

Fig. 16. Rotor speed of generator at $\mu = 0.8$ (without controller and with the nominal value of AVR gain $K_R = 200$)

Fig. 17 and 18 show the time history of the system when the nonlinear controller is included with a gain $K = 5000$ together with a small value of AVR gain $K_R = 2$ at $\mu = 0.8$ after 2.5% initial disturbance on the rotor speed of generator. It can be observed that the nonlinear controller together with small AVR gain stabilizes the system.

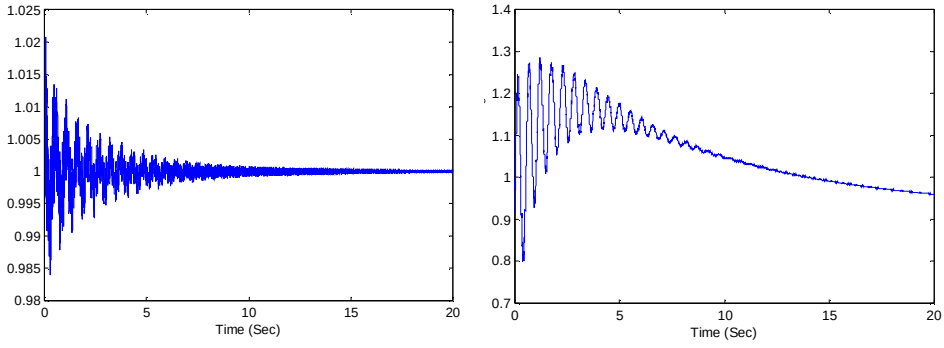

Fig. 17. Closed loop response (a) Rotor speed, (b) Rotor angle of generator at μ=0.8 after 2.5% initial disturbance on the rotor speed of generator (with a nonlinear state feedback controller gain $K = 5000$ and AVR gain $K_R = 2$)

Finally, fig. 18 shows the time history of the nonlinear control signal.

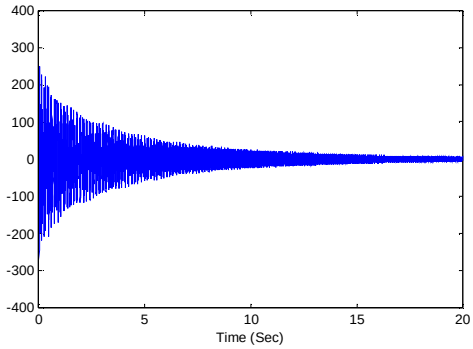

Fig. 18. Time history of the nonlinear controller at $\mu = 0.8$ after 2.5% initial disturbance on the rotor speed of generator

6 Conclusions

Linear and nonlinear state feedback controllers are used to control the chaotic oscillations and bifurcations of the IEEE second benchmark model of SSR. Both controllers succeeded to change unstable attractor to a stable one. Linear state feedback controller gives better response for initial disturbance but in a very narrow region of compensation factor, while nonlinear controller together with small AVR gain stabilize the operating point of the system at all realistic compensation factors, and hence canceling all bifurcations of the system.

7 Appendix

Numerical Parameters:

a) Synchronous Generator (in pu, on the base of its ratings):

$X_{ffd} = 1.6286$ $X_{afd} = 1.5100$ $X_{fkd} = 1.5100$

$r_{fd} = 0.00096$ $X_{d} = 1.6500$ $X_{akd} = 1.5100$

$r_{a} = 0.0045$ $X_{q} = 1.5900$ $r_{kd} = 0.0160$

$X_{akq} = 1.4500$ $X_{kkd} = 1.6420$ $X_{kkq} = 1.5238$

$r_{kq} = 0.0116$

b) Network (Transmission line, in pu on the base of generator ratings):

$X_T = 0.1200$ $X_{L1} = 0.4800$ $X_b = 0.1800$

$R_b = 0.0084$ $R_T = 0.0012$ $R_1 = 0.0444$

$R_2 = 0.0402$ $X_{L2} = 0.4434$

c) Mechanical system (in pu on the base of the generator ratings):

$M_1 = 0.0138$ $D_1 = 0.0014$ $K_{1g} = 3.7363$

$M_g = 1.7581$ $D_g = 0.1758$ $K_{g2} = 83.3823$

$M_2 = 3.1004$ $D_2 = 0.3100$ $K_{23} = 42.6572$

$M_3 = 0.4980$ $D_3 = 0.0498$

d) AVR and PSS:

$K_R = 200$ $T_R = 0.025\,\mathrm{s}$ $T_W = 10\mathrm{s}$

$K_s = 12$ $T_1 = 0.048\mathrm{s}$ $T_2 = 0.032\mathrm{s}$

References

1. Begamudre R.D. *Extra High Voltage A.C Transmission Engineering,* New Age International (P) Limited, New Delhi, 1997
2. Zhu W., Mohler R.R., Spce R., Mittelstadt W.A., Maratukulam D. Hopf Bifurcation in a SMIB Power System with SSR, *IEEE Trans. on Power Systems,* **11**(3), p. 1579–1584, 1996
3. Nayfeh A.H., Harb A.M., Chin C.-M., Hamdan A.M.A., Mili L., Application of Bifurcation Theory to Subsynchronous Resonance in Power Systems, *International Journal of Bifurcation and Chaos,* **8**(1), p. 157–172, 1998
4. Harb A.M., Mili L., Nayfeh A.H., Chin C.-M. On the Effect of the Machine saturation on SSR in Power Systems, *Electric Machines and Power Systems,* **28**, p. 1019–1035, 2000
5. Tesi A., Abed E.H., Genesio R., Wang H.O. Harmonic Balance Analysis of Period-Doubling Bifurcations with Implications for Control of Nonlinear Dynamics, *Automatica,* **32**, p. 1255–1271, 1996
6. Wang H.O., Abed E.H. Bifurcation Control of a Chaotic Systems, *Automatica*, **31**, p. 1213–1226, 1995

7. Abed E.H. Bifurcation-Theoretic Issues in the Control of Voltage Collapse, In: *Proc. IMA Workshop on Systems and Control Theory for Power Systems*, Chow J.H., Kokotovic P.V., Thomas R.J. (Eds.), Springer, p. 1–21, 1995

8. Chen D., Wang H.O., Chen G. Anti-Control of Hopf Bifurcations Through Washout Filters, In: *Proc. 37th IEEE Conf. Decission and Control*, Tampa, FL, Dec., 16–18, p. 3040–3045, 1998

9. Chen G., Dong X. *From Chaos to Order: Methodologies, Perspectives and Applications*, World Scientific, Singapore, 1998

10. Moiola J.L., Chen G. *Hopf Bifurcation Analysis: A Frequency Domain Approach*, World Scientific, Singapore, 1996

11. Abed E.H., Fu J.H. Local Feedback Stabilization and Bifurcation Control, I. Hopf Bifurcation, *Syst. Cont. Lett.*, **7**, p. 11–17, 1986

12. Laufenberg M.J., Pai M.A., Padiyar K.R. Hopf Bifurcation Control in Power Systems with Static VAR Compensator, *Int. J. Elect. Power and Energy Syst.*, **19**, p. 339–347, 1997

13. Calandrini G., Paolini E., Moiola J.L., Chen G. Controlling Limit Cycles and Bifurcations, *Controlling Chaos and Bifurcations in Engineering Systems*, C. Chen G. (Ed.), CRC Press, p. 200–227, 1999

14. Berns D.W., Moiola J.L., Chen G. Feedback Control of Limit Cycle Amplitude from a Frequency Domain Approach, *Automatica*, **34**, 1567-1573, 1998

15. Cam U., Kuntman H. A New CCII-Based Sinusoidal Oscillator Providing Fully Independent Control of Oscillation Condition and Frequency, *Microelectron. J.*, **29**, p. 913–919, 1998

16. Basso M., Evangelisti A., Genesio R., Tesi A. On Bifurcation Control in Time Delay Feedback Systems, *Int. J. Bifurcation and Chaos*, **8**, p. 713-721, 1998

17. Alhumaizi K., Elnashaie S.E.H. Effect of Control Loop Configuration on the Bifurcation Behavior and Gasoline Yield of Industrial Fluid Catalytic Cracking (FFC) Units, *Math. Comp. Modelling*, **25**, p. 37–56, 1997

18. Moiola J.L., Desages A.C., Romagnoli J.A. Degenerate Hopf Bifurcation via Feedback System Theory-Higher Order Harmonic Balance, *Chem. Eng. Sci.*, **4**, p. 1475–1490, 1991

19. Liaw D.C., Abed E.H. Control of Compressor Stall Inception – A Bifurcation-Theoretic Approach, *Automatica*, **32**, p. 109–115, 1996

20. Gu G., Sparks A.G., Banda S.S. Bifurcation Based Nonlinear Feedback Control for Rotating Stall in Axial Flow Compressors, *Int. J. Cont.*, **6**, p. 1241–1257, 1997

21. Ono E., Hosoe S., Tuan H.D., Doi S. Bifurcation in Vehicle Dynamics and Robust Front Wheel steering Control, *IEEE Trans. Contr. Syst. Technol.*, **6**, p. 412–420, 1998

22. Dobson I., Lu L.M., Computing an Optimal Direction on Control Space to Avoid Saddle-Node Bifurcation and Voltage Collapse, In: *Electric Power Systems, IEEE Trans. Auto. Cont.*, **37**, p. 1616–1620, 1992

23. Goman M.G., Khramtsovsky A.V. Application of Continuation and Bifurcation Methods to the Design of Control systems, *Phil. Trans. R. Soc. Lond.*, **A356**, p. 2277–2295, 1998

24. Moroz I.M., Baigent S.A., Clayton F.M., Lever K.V. Bifurcation Analysis of the Control of an Adaptive Equalizer, In: *Proc. R. Soc. London, Series A-Math. And Phys. Sciences*, **537**, p. 501–515, 1992

25. Senjyu T., Uezato K. Stability Analysis and Suppression Control of Rotor Oscillation for Stepping Motors by Lyapunov Direct Method, *IEEE Trans. Power Electron*, p. 333–339, 1995

26. Srivastava K.N., Srivastava S.C. Application of Hopf Bifurcation Theory for Determining Critical Value of a Generator Control or Load Parameter, *Int. J. Electrical Power Energy Syst.*, **17**, p. 347–354, 1995

27. Ueta T., Kawakami H., Morita I. A Study of the Pendulum Equation With a Periodic Impulse Force-Bifurcation and Chaos, *IEICE Trans. Fundam Electr. Commun. Comput. Sci. E78A*, p. 1269–1275, 1995

28. Volkov A.N., Zagashvili U.V. A Method of Synthesis for Automatic Control Systems with Maximum Degree of Stability and Given Oscillation Index, *J. Comput. Systs. Sci. Int.*, **36**, p. 29–34, 1997

29. Hassard B., Jiang K. Unfolding a Point of Degenerate Hopf Bifurcation in an Enzyme-Catalyzed Reaction Model, *Siam J. Math. Anal.*, **23**, p. 1291–1304, 1992

30. Hu G., Haken H. Potential of the FokkerPlank Equation at Degenerate Hopf Bifurcation Points, *Phys. Rev.* **A41**, p. 2231–2234, 1990

31. Iida S.K., Ogawara K., Furusawa S.A. Study on Bifurcation Control Using Pattern Recognition of Thermal Convection, *JSME Int. J. Series B-Fluid and Thermal Eng.*, **39**, p. 762–767, 1996

32. Reznik D., Scholl E. Oscillation Modes, Transient Chaos and its Control in Modulation-Doped Semi-Conductor Double-Heterostructure, *Zeitschrift fur physik B-Condensed matter*, **91**, p. 309–316, 1993

33. Malmgren B.A., Winter A., Chen D.L. El Nino Southern Oscillation and North Atlantic Oscillation Control of Climate in Puerto Rico, *J. Climate*, **11**, p. 2713–2717, 1998

34. Abed E.H., Wang H.O., Chen R.C. Stabilization of Period Doubling Bifurcations and Implications for Control of Chaos, *Physica. D70*, p. 154–164, 1994

35. Yabuno H. Bifurcation Control of Parametrically Excited Duffing System By a Combined Linear-Plus-Nonlinear Feedback Control, *Nonlin. Dyn.*, **12**, p. 264–274, 1997

36. Harb A.M., Widyan M.S. Chaos and Bifurcation as Applied to Subsynchronous Resonance of the IEEE Second Benchmark Model, submitted to *Electric Power Components and Systems*.

37. Saadat H. *Power System Analysis,* McGraw Hill, 1999